Design of Circular Log-Periodic Arrays Using Electromagnetic Simulations

Özgür Ergül and Levent Gürel*
Department of Electrical and Electronics Engineering
Bilkent University, TR-06800, Bilkent, Ankara, Turkey
E-mail: ergul@ee.bilkent.edu.tr, lgurel@bilkent.edu.tr

Introduction

We consider the design of circular arrays of log-periodic (LP) antennas by taking advantage of a powerful electromagnetic simulation environment. We model the antennas by using perfectly conducting sheets and apply the electric-field integral equation (EFIE) to solve the radiation problem in the frequency domain. The simultaneous discretization of the geometry and the integral equation leads to a matrix equation, which is solved by an iterative method employing the multi-level fast multipole algorithm (MLFMA). The excitations of the antennas in the circular arrays are optimized by the genetic algorithms to add a beam-steering ability to the arrays. Results of two different types of array configurations are presented to demonstrate their broadband and beam-steering properties.

Simulation of LP Antennas

Fig. 1 depicts a trapezoidal-tooth LP antenna, which is designed for a broadband operation in the 300–800 MHz range [1],[2]. The antenna has two arms, each of which is 1 m long and separated by 45°. There are 38 elements on each arm and the geometric growth factor (τ) of the antenna is 0.95 so that

$$\tau = \frac{R_{i+1}}{R_i} = 0.95, \quad i = 1, ..., 37, \tag{1}$$

where R_i represents the length of the ith element and $R_1 = 27$ cm. LP antennas and their arrays are modelled with perfectly conducting sheets with zero thickness. The radiation problem in the frequency domain is formulated by the EFIE [3], derived from the boundary condition for the tangential electric field on the surface. Applying a simultaneous discretization on the geometry and the EFIE, we obtain the $N \times N$ matrix equation

$$\sum_{n=1}^{N} Z_{mn}^{E} a_n = v_m^{E}, \qquad m = 1, ..., N, \tag{2}$$

where

$$Z_{mn}^{E} = \int_{S_m} d\boldsymbol{r}\ \boldsymbol{t}_m(\boldsymbol{r}) \cdot \int_{S_n} d\boldsymbol{r'} \left[\overline{\boldsymbol{I}} + \frac{\nabla\nabla}{k^2} \right] g(\boldsymbol{r}, \boldsymbol{r'}) \cdot \boldsymbol{b}_n(\boldsymbol{r'}) \tag{3}$$

represents the matrix element and v_m^E is the excitation vector. As the basis ($\boldsymbol{b}_n$ on S_n) and testing ($\boldsymbol{t}_m$ on S_m) functions, we employ the Rao-Wilton-Glisson [4] functions defined on planar triangles. The solution of (2) is performed by an iterative algorithm, where the

This work was supported by the Turkish Academy of Sciences in the framework of the Young Scientist Award Program (LG/TUBA-GEBIP/2002-1-12), by the Scientific and Technical Research Council of Turkey (TUBITAK) under Research Grant 103E008, and by contracts from ASELSAN and SSM.

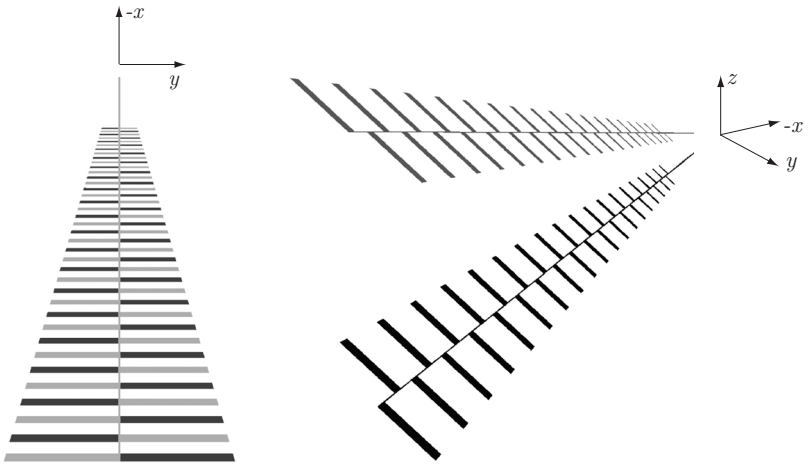

Fig. 1. Trapezoidal-tooth LP antenna. (a) Top view, (b) three-dimensional view. This antenna is employed to construct the circular arrays.

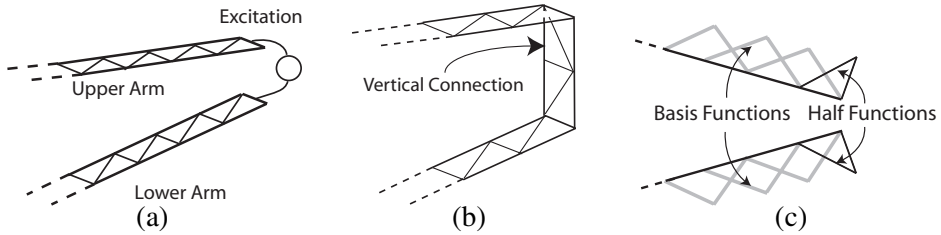

Fig. 2. (a) Feed location of an LP antenna. (b) Vertical connection to implement a delta-gap source. (c) Half basis functions to model a current source without a vertical connection.

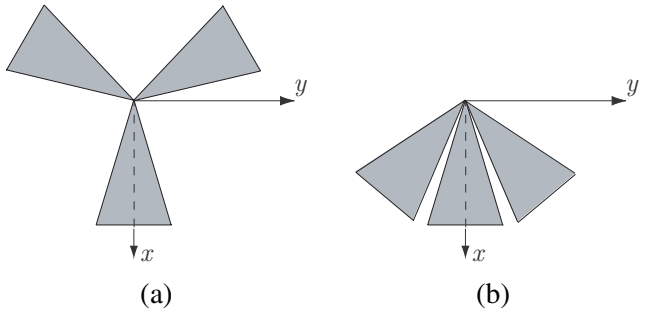

Fig. 3. Circular arrays of three LP antennas. (a) Circular-symmetric array, (b) circular-sectoral array.

matrix-vector products are accelerated by the MLFMA [5]. After finding the coefficients a_n in (2), the radiation intensity of the antenna is calculated as

$$f(\theta,\phi) = \frac{k^2\eta^2}{4\pi}\left|\hat{\theta}\hat{\theta}\cdot\boldsymbol{F}(\theta,\phi) + \hat{\phi}\hat{\phi}\cdot\boldsymbol{F}(\theta,\phi)\right|^2, \tag{4}$$

where $\boldsymbol{F}(\theta,\phi)$ represents the vector current moment.

Fig. 2(a) depicts the feed location of an LP antenna, where the two arms of the antenna become close to each other. For a proper representation of the feed, there are two techniques as sketched in Figs. 2(b) and (c). In the first case [Fig. 2(b)], the arms of the antenna are connected by a vertical strip, on which a delta-gap source is defined. In the second case [Fig. 2(c)], the arms are not connected physically, but instead, a source

and a sink created by a pair of half basis functions are defined at the opposite arms of the antenna. In this manner, the combination of the source and the sink simulates a current source feeding the antenna.

Design of Circular LP Arrays

In this paper, we consider two types of circular LP arrays as depicted in Fig. 3, where the LP antennas are arranged in circular configurations. In the first type [Fig. 3(a)], the antennas are located symmetrically. In the second type [Fig. 3(b)], the antennas are close to each other and the array spans a sector of the circle. Theoretically, either one of these circular arrays of the LP antennas should preserve the broadband characteristics. On the other hand, it is known that the mutual couplings between the antennas affect the radiation characteristics significantly and deteriorate the frequency independence [1].

In the process of designing the arrays in Fig. 3, we desire to optimize the complex excitations of the antennas to maximize the directive gain defined as

$$D(\theta,\phi) = 4\pi \frac{f(\theta,\phi)}{P(\theta,\phi)}, \qquad P(\theta,\phi) = \int_0^{2\pi} \int_0^{\pi} f(\theta,\phi) \sin\theta d\theta d\phi, \tag{5}$$

where $f(\theta,\phi)$ represents the radiation intensity derived in (4). Optimization of the directive gain has two consequences. First, the radiation characteristics are further stabilized with respect to the frequency. Second, the arrays are equipped with the beam-steering ability. Due to the large optimization space, we employ the genetic algorithms to find the optimal complex excitations providing the maximum directive gain in the desired direction. For the array in Fig. 3(a), we perform only one MLFMA solution for each frequency. Then, the optimization algorithm optimizes the excitations by employing symmetry and superposition. For the array in Fig. 3(b), three solutions are required for each frequency, where the three antennas are excited one by one.

Figs. 4 and 5 present the results of the optimizations. In Fig. 4, the optimized far-field radiation patterns are plotted for two different frequencies and for different array configurations shown at the bottom. In all cases, the directive gain in the $-x$ direction is optimized. For the second and fourth configurations, the arrays are rotated, so that the beam steering is achieved for 30°. In Fig. 5, the optimized directive gain in the $-x$ direction is plotted with respect to the frequency for the two arrays in Fig. 3.

Concluding Remarks

The optimization results in Figs. 4 and 5 lead to the following conclusions:

1) The circular-symmetric array in Fig. 3(a) provides relatively lower directive gain and narrower beam steering. For 30° rotation, the directive gain falls below 6 and the main beam cannot be preserved in the $-x$ axis, i.e., the main beam cannot be steered 30° by adjusting the excitations of the antennas. However, the symmetry of this array creates an advantage since the steerable sector can be rotated by the exchange of the excitations among the antennas. Therefore, this array provides three distinct narrow sectors for the beam steering.
2) The circular-sectoral array in Fig. 3(b) provides relatively higher directive gain and wider range for beam steering. The beam can be steered up to 50° with directive gain of 10. However, there is a single steerable sector.

We conclude that both types of the arrays have specific advantages that may render them more preferable depending on the application.

References

[1] Ö. Ergül and L. Gürel, "Log-periodic antenna design using electromagnetic simulations," in *Proc. IEEE Antennas and Propagation Soc. Int. Symp.*, vol. 1, pp. 245–248, 2003.

[2] Ö. Ergül and L. Gürel, "Nonplanar trapezoidal-tooth log-periodic antennas: design and electromagnetic modelling," *Radio Science*, vol. 40, Oct. 2005.

[3] A. W. Glisson and D. R. Wilton, "Simple and efficient numerical methods for problems of electromagnetic radiation and scattering from surfaces," *IEEE Trans. Antennas Propagat.*, vol. AP-28, no. 5, pp. 593–603, Oct. 1980.

[4] S. M. Rao, D. R. Wilton, and A. W. Glisson, "Electromagnetic scattering by surfaces of arbitrary shape," *IEEE Trans. Antennas Propagat.*, vol. AP-30, pp. 409–418, May 1982.

[5] C.-C. Lu and W. C. Chew, "Multilevel fast multipole algorithm for electromagnetic scattering by large complex objects," *IEEE Trans. Antennas Propagat.*, vol. 45, no. 10, pp. 1488–1493, Oct. 1997.

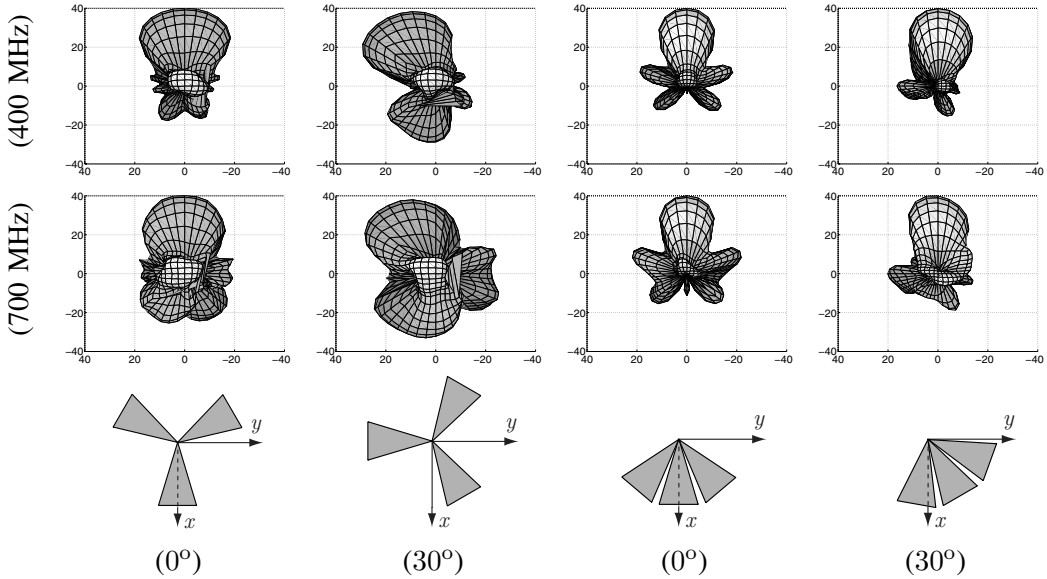

Fig. 4. Normalized far-field radiation of the arrays in Fig. 3 for various frequencies and configurations. The directive gain is optimized in the $-x$ direction.

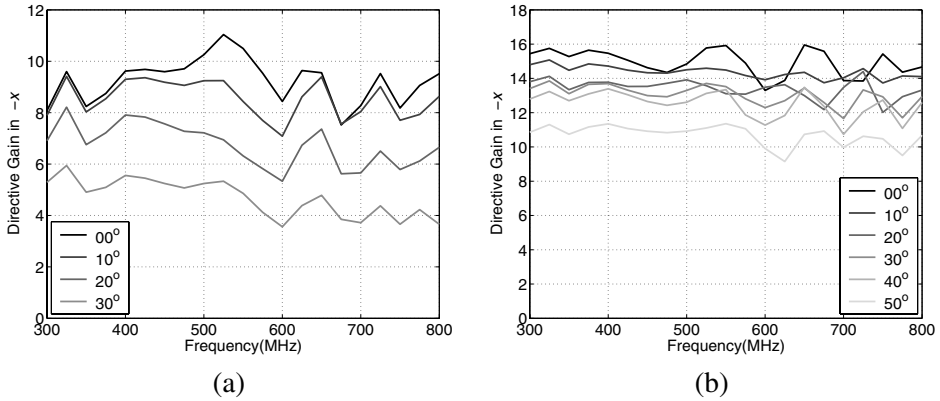

Fig. 5. Directive gain in the $-x$ direction for the arrays in (a) Fig. 3(a) and (b) Fig. 3(b) obtained by the optimization at various frequencies and for different rotations of the arrays.